A kinetic compass for the design of experiments to determine kinetic parameters

Matteo Krüger
Max Planck Institute for Chemistry
Ashmi Mishra
Max Planck Institute for Chemistry
Peter Spichtinger
Johannes Gutenberg University
Ulrich Pöschl
Max Planck Institute for Chemistry
Thomas Berkemeier
t.berkemeier@mpic.de

Max Planck Institute for Chemistry

Research Article

Keywords: Chemical Kinetics, Experiment Design, Global Optimization, Inverse Problem, Ensemble Methods, Multiphase Chemistry, Machine Learning

Posted Date: September 6th, 2023

DOI: https://doi.org/10.21203/rs.3.rs-3317747/v1

Additional Declarations: No competing interests reported.

Version of Record: A version of this preprint was published at Journal of Cheminformatics on March 22nd, 2024. See the published version at https://doi.org/10.1186/s13321-024-00825-0.

A kinetic compass for the design of experiments to determine kinetic parameters

Matteo Krüger[1], Ashmi Mishra[1], Peter Spichtinger[2], Ulrich Pöschl[1], Thomas Berkemeier[1*]

[1*]Multiphase Chemistry Department, Max Planck Institute for Chemistry, Hahn-Meitner-Weg 1, Mainz, 55128, Rhineland Palatinate, Germany.
[2]Institute for Atmospheric Physics, Johannes Gutenberg University, Johann-Joachim-Becher-Weg 21, Mainz, 55128, Rhineland Palatinate, Germany.

*Corresponding author(s). E-mail(s): t.berkemeier@mpic.de;
Contributing authors: m.krueger@mpic.de; a.mishra@mpic.de; spichtin@uni-mainz.de; u.poschl@mpic.de;

Abstract

Kinetic process models are widely applied in science and engineering, including atmospheric, physiological and technical chemistry, reactor design, or process optimization. These models rely on numerous kinetic parameters such as reaction rate, diffusion or partitioning coefficients. Determining these parameters by experiments can be challenging, especially for multiphase systems, and researchers often face the task of intuitively selecting experimental conditions to obtain insightful results. We developed a kinetic compass (KC) method that integrates kinetic models, global optimization, ensemble methods, and machine learning to identify experimental conditions with the greatest potential to constrain kinetic parameters. The approach is based on the quantification of model output variance in an ensemble of solutions that agree with experimental data. The utility of the KC method is demonstrated for the kinetic parameters in a multi-layer model describing the heterogeneous ozonolysis of oleic acid aerosols. We show how neural network surrogate models of the multiphase chemical reaction system can be used to accelerate the application of the kinetic compass for a comprehensive mapping and analysis of experimental conditions. The code is openly available and can be adapted to various types of process models.

Keywords: Chemical Kinetics, Experiment Design, Global Optimization, Inverse Problem, Ensemble Methods, Multiphase Chemistry, Machine Learning

1 Introduction

In multiphase chemical kinetics, the rate of change in complex systems can be described by resolving mass transport and chemical reactions at the molecular process level [1, 2]. While the underlying physical and chemical principles are well understood, the individual processes are inherently coupled and the chemical and physical parameters, such as reaction, diffusion, or partitioning coefficients, are often unknown or poorly constrained [3, 4]. The integration of these processes occurring in parallel or in sequence often requires

computational kinetic models (KM). KM return the concentration time profiles of reactants or products under specified environmental or experimental conditions [5–10]. However, the input parameters for KM may not be known *a priori*, and their determination can be challenging [11–14]. The deduction or constraint of model input parameters from model output is known as solving the inverse problem. In practice, researchers often utilize statistical approaches to solve the inverse problem with global optimization techniques [15–18]. Such techniques determine sets of parameter values, so-called fits, that lead to model outputs in agreement with previously acquired experimental data. In ill-posed problems, Berkemeier et al. 2021 [19] proposed the consideration of ensembles of sufficiently well-fitting parameter sets to extract information from the corresponding range of kinetic model solutions in underdetermined optimization problems. All kinetic parameter sets in such a *fit ensemble* represent valid solutions that match the experiments taken into account, within a specified error margin.

Surrogate models (SM) are machine learning models that are trained on inputs and outputs of a template model. A SM can be used to substitute the template model in applications that benefit from low computational cost in exchange for slightly increased model uncertainty. Satisfactory model accuracy can be ensured by a sufficient size of the training data set, and therefore depends on the initial investment of computational resources [20]. SM have helped solving the issue of computational cost in many fields of research, e.g. in geoscientific and atmospheric modelling [21–27], chemical process engineering [28], water resources modelling [29, 30], or optimization in supply chain management [31]. SM can also aid inverse modelling approaches. Berkemeier et al. 2023 [20] showed that SM-supported fit ensemble acquisition greatly outperforms regular sampling with the kinetic multi-layer model of aerosol surface and bulk chemistry (KM-SUB) [5] in terms of acquired fits for a given computational effort. However, it remains unclear how SM uncertainty affects the reliability of inverse modelling techniques.

Among model input parameters, we differentiate between kinetic parameters that define the physical and chemical properties of the modelled system (e.g. reaction rate coefficients), and parameters that define the environmental or experimental conditions (e.g. initial concentrations or temperature). When a model is evaluated for experimental conditions that differ from those for which its kinetic parameters were derived, model uncertainty may strongly increase [2]. This situation may arise in particular when the data underlying the model is limited, or when conditions in the laboratory experiment (e.g. a test reactor) deviate from the real-world application of interest (e.g. the atmosphere, an industrial plant, or an engine). Furthermore, when extrapolating a model to conditions outside its calibration range, not all fits in a fit ensemble may behave in the same way. This ensemble variance associated with a fit ensemble can be used to assess the model's fit uncertainty over a range of experimental conditions [19]. The ensemble variance at a specific set of experimental conditions may also be an indicator for parameter sensitivity, and of the potential to constrain the model if experimental data was available for these conditions. Thus, while data from any additional experiment may decrease the fit uncertainty of an associated model, this process can be optimized by selecting experimental conditions associated with high ensemble variance. These conditions are most likely to constrain the underlying model and its physical and chemical parameters.

For experimenters, it is difficult to guess such optimal conditions *a priori*. In the fields of engineering and materials science, so-called calibration experiment design optimization techniques optimize experimental inputs to maximize the information obtained with a limited testing budget [32–34]. However, to our knowledge, there are no general, quantitative tools available that utilize kinetic process models to guide laboratory experiments. In this study, we present the kinetic compass (KC), a method that optimizes the selection of future laboratory experiments to minimize a model's fit uncertainty. The KC is used alongside the kinetic multi-layer model of aerosol surface and bulk chemistry (KM-SUB), and a neural network SM for it, to demonstrate its functionality in experiment design and inverse modelling.

2 Method

We present the kinetic compass (KC), a method for experiment prioritization and reduction of a model's fit uncertainty. The method requires a process model, data from previous laboratory experiments, and a set of variable experimental parameters that describe future experiments of interest. The individual steps of the proposed workflow are displayed in Fig. 1.

2.1 Inverse modelling solutions and uncertainty

The KC can be described as a method for uncertainty quantification. A kinetic model's uncertainty can be based on model inadequacy, i.e. lack of knowledge of the underlying physics or chemistry, or model parametric uncertainty, i.e. insufficient knowledge of its input parameters. Parametric uncertainty is caused by the coupled nature of parameters and by underdetermination of the modelled system. To estimate parametric uncertainty, inverse modelling can be extended to an ensemble of kinetic parameter sets that return sufficient agreement with multiple experimental data sets [15, 19]. All possible sets of chemical and physical parameter values that lead to a sufficiently low residual between model output and experimental data, so-called fits, form the solution space of a kinetic model. In practice, we use a finite collection of fits, referred to as *fit ensemble*, as representation of the model solution space. Additional experimental data can help to narrow down the fit ensemble and thus decrease model parametric uncertainty.

2.2 Operating principle

The KC is a framework to optimize the deduction or constraint of kinetic parameters with experiments. In general, the information gained from new experimental data can be used to reject fits from a fit ensemble. The KC finds experimental conditions with the highest constraint potential, optimizing the reduction of model solution space and model parametric uncertainty. For this purpose, the method computes ensemble solutions under experimental conditions that have not been considered previously, and determines the ensemble variance under these conditions. We present two metrics evaluating the ensemble variance, the *ensemble spread* of model solutions (Sect. 2.3) and the *parameter (boundary) constraint potential* (Sec. 2.4). By sampling the space of feasible experiments, *constraint potential maps* (Sec. 2.5) of these metrics are obtained. Maxima on these maps represent prospective experiments that are most likely to achieve large constraints of the model. After fit ensemble filtering based on the new experimental data, the KC method can be repeated to suggest the next experiment. In this study, we simulate the suggested laboratory experiments with the model KM-SUB to showcase the alternating application of the KC with laboratory experiments. For more detailed and mathematical definitions of process models, their solution space, as well as fit ensembles and ensemble solutions, see Suppl. Note 1. For the specifications of fit ensemble acquisition and error calculation in this study, see Suppl. Note 2.

2.3 Ensemble spread

The ensemble spread is a measure for the variance between a multitude of model predictions. Resembling similar concepts in weather and climate forecasting [35], we calculate the ensemble spread (ES) as:

$$\mathrm{ES} = \frac{\int(\overline{Z}(x) + \sigma_Z(x))dx - \int(\overline{Z}(x) - \sigma_Z(x))dx}{\int \overline{Z}(x)dx} \tag{1}$$

where $(x_m)_{m=1,\dots,n_z}$ is the sequence of independent variables associated with the output sequence $(z_m)_{m=1,\dots,n_z}$, and $\int \overline{Z}$, $\int \overline{Z} + \sigma$ and $\int \overline{Z} - \sigma$ are integrals of the interpolated sequences $(\overline{Z_m})_{m=1,\dots,n_z}$, $(\overline{Z_m} + \sigma_m)_{m=1,\dots,n_z}$ and $(\overline{Z_m} - \sigma_m)_{m=1,\dots,n_z}$ for n_z model outputs with an ensemble mean $\overline{Z_m}$ and ensemble standard deviation σ_m (Suppl. Note 3).

In short, the ensemble spread describes the area enclosed by the curves of the ensemble mean $\pm$ its standard deviation, normalized by the area under the ensemble mean curve. Visualizations of the ensemble spread as constraint potential metric are provided in Fig. 2D,E. A large ensemble spread is generally associated with a larger fraction of rejected fits during fit ensemble filtering.

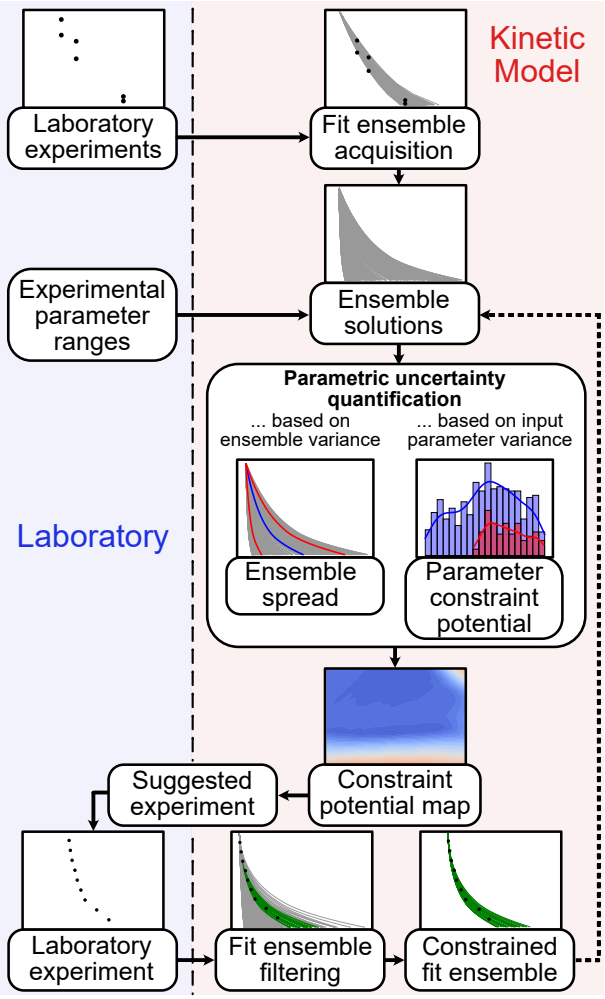

Fig. 1 Workflow of the kinetic compass (KC) method presented in this study. The method relies on exchange between laboratory experiments (left) and model calculations (right) to eliminate variance in model output. Data from laboratory experiments are used for the acquisition of a fit ensemble, which are kinetic parameter sets that lead to model outputs in agreement with the experimental measurements. Evaluating the model for the entire fit ensemble and over a defined range of experimental parameters yields sets of ensemble solutions that serve as the basis for all calculations with the KC. The KC offers two metrics for parametric uncertainty quantification: ensemble spread, and parameter (boundary) constraint potential (Sec. 2.4). The metrics are used to build constraint potential maps, which highlight areas with large model output variance in the experimental parameter range. These experimental parameters are suggested as next experiment as they are likely to lead to rejection of a large number of fits during fit ensemble filtering. The KC can be used iteratively (dashed arrow), using the ensemble solutions of the constrained fit ensembles.

2.4 Parameter boundary constraint potential

The parameter (boundary) constraint potential allows an extension of the method to constraints of individual kinetic parameters. The metric quantifies the potential narrowing of an individual parameter's boundaries in the constrained fit ensemble.

In brief, the parameter constraint potential is calculated by iterating over predictions in an ensemble solution. In each iteration, we calculate the distribution of remaining kinetic parameters in a hypothetical constrained fit ensemble that would be obtained if one selected fit of the ensemble would represent the truth. The kinetic parameter's boundaries in this distribution are normalized by its current boundaries in the fit ensemble to

compute a numerical value for the parameter's constraint potential.

To calculate the parameter (boundary) constraint potential, we determine the subset C of the fit ensemble FE. C contains all fits that lead to model solutions within error threshold θ in comparison to the model solution of subset-forming fit FE_l:

$$\mathrm{C}_l = \{\mathrm{FE}_r : \Delta(\mathrm{ENS}_l, \mathrm{ENS}_r) < \theta\} \quad (2)$$

where ENS_l and ENS_r are the model solutions using fits FE_l and FE_r in the evaluated ensemble solution (ENS). Hence, we obtain one subset C_l for each selected subset-forming fit FE_l. If every fit is evaluated as subset-forming fit in turn, n_{FE} subsets are generated for every ensemble solution. The parameter constraint potential (CP) for a specific parameter λ_p and ensemble solution is then defined as:

$$\mathrm{CP}_p = \sum_{l=1}^{n_{\mathrm{FE}}} (\mathrm{Q}\mathit{10}_{\lambda_p,l} - \min(\lambda_p)) + (\max(\lambda_p) - \mathrm{Q}\mathit{90}_{\lambda_p,l}) \quad (3)$$

where $\mathrm{Q}\mathit{10}_{\lambda_p,l}$ and $\mathit{90}_{\lambda_p,l}$ are the 10- and 90-percentiles of the distribution of λ_p in subset C_l, respectively. $\min(\lambda_p)$ and $\max(\lambda_p)$ are the global minimum and maximum of the selected kinetic parameter in the entire fit ensemble.

Note that the computational effort associated with this method is large due to the pairwise comparison of all predictions in an ensemble solution. Therefore, we suggest an approximation based on a reduced sample density. A detailed definition of the parameter constraint potential with reduced sample density is presented in Supplementary Note 4 and visualized in Fig. S4.

2.5 Constraint potential maps

The application of a metric for model constraint potential on a range of ensemble solutions (one for each tested experimental condition) can be visualized in a constraint potential map. This map is a n-dimensional hypersurface, where n is the number of varied experimental parameters, and whose maxima represent experimental conditions favorable for constraint of the underlying model. An example for a constraint potential map is presented for two varied experimental parameters and the ensemble spread metric in Fig. 2. For further information on the chemical system (oleic acid ozonolysis) and the variable experimental parameters (particle radius, ozone concentration), as well as a description of the restrictions regarding experimental accessibility applied in this work, see Sec. 2.6, Suppl. Note 5, and Fig. S5. Note that while we evaluate a full grid of combinations of experimental parameters for the purpose of testing and visualization, the constraint potential metrics can similarly be used with an optimization algorithm to reduce the required computational effort.

2.6 Kinetic multi-layer model and neural network surrogate model

In this study, we use the kinetic multi-layer model of aerosol surface and bulk chemistry (KM-SUB) [5] along with experimental data of the heterogeneous ozonolysis of oleic acid from the literature. However, the KC method can be used with any process model and underlying chemical or physical system. Detailed information about KM-SUB can be found in previous publications [5, 12]. In brief, KM-SUB is a chemical flux model that explicitly describes gas diffusion, accommodation of gas molecules to surfaces, surface-bulk exchange, bulk diffusion, as well as chemical reaction at the surface and in the bulk of a condensed phase. The resulting set of ordinary differential equations is solved numerically. KM-SUB input parameters include initial concentrations, chemical reaction rate coefficients, and mass transport coefficients, and are presented in Table 1. KM-SUB outputs are the concentration profiles over space and time for all chemical species.

For the training of neural network surrogate models, KM-SUB output is simplified to nine points of reaction progress, i.e. the time required to reach 90 %, 80 %, 70 %, 60 %, 50 %, 40 %, 30 %, 20 % and 10 % of the total number of oleic acid (OL) in a single aerosol particle, $N_{\mathrm{OL},0}$. For comparability, we represent the output of the full KM-SUB model in this study in the same way. We train a fully-connected, feed-forward neural network on 1×10^6 KM-SUB outputs as training data. For further information on training of the surrogate model see Berkemeier et al. 2023 [20] and Suppl. Note 6.

The KC method requires evaluation of the underlying process model during fit ensemble acquisition and during calculation of ensemble

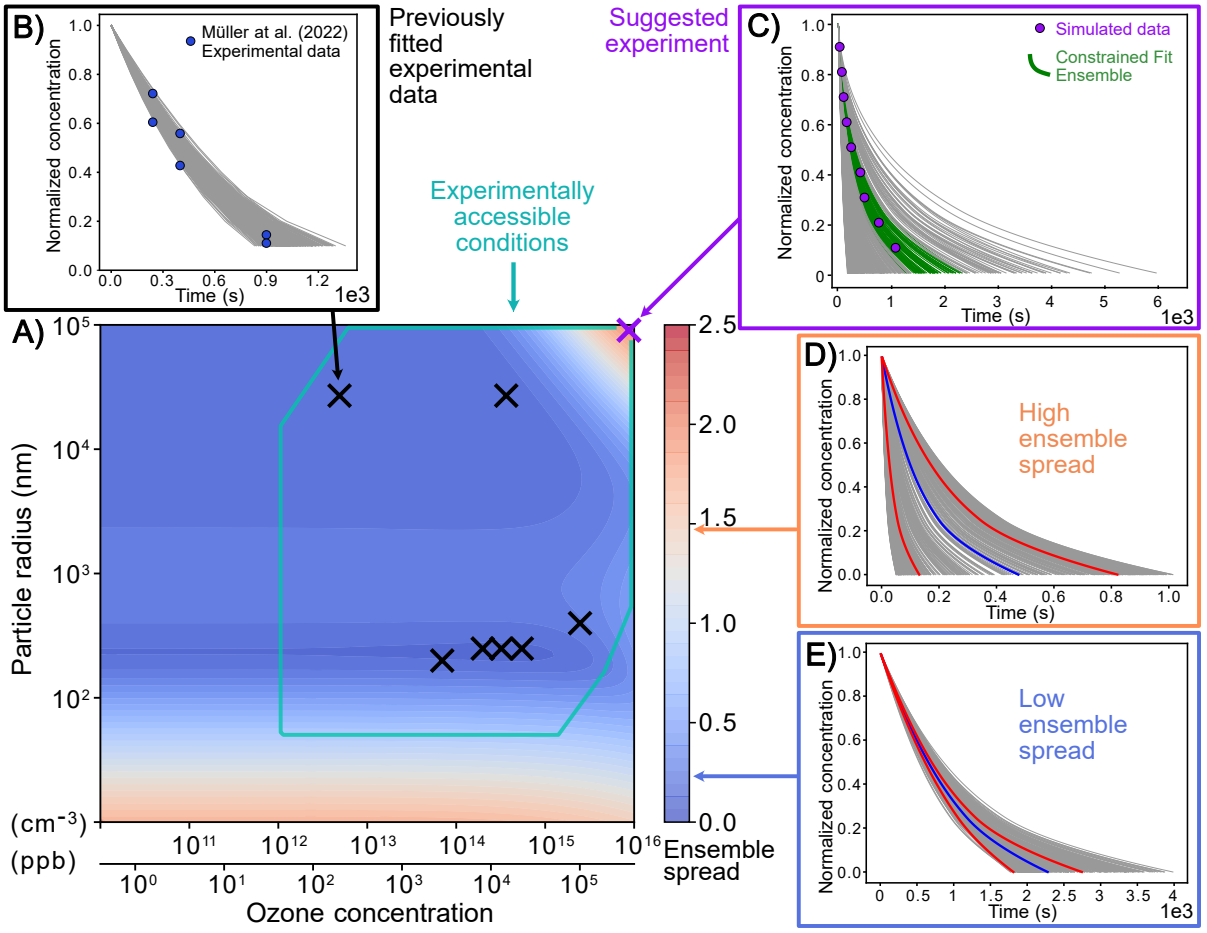

Fig. 2 Constraint potential map obtained with the kinetic compass (KC) method. The contour map in (A) shows an exemplary constraint potential map using the ensemble spread metric. Model calculations are obtained with KM-SUB on a 100×100 grid of two experimental parameters, ozone concentration and particle radius, and for a fit ensemble of 500 fits. The teal box frames the area of experimentally accessible conditions with regards to particle radius, ozone concentration and predicted experiment duration (Suppl. Note 5). Black crosses in (A) mark the experimental conditions of available experimental data that were used to obtain the fit ensemble (cf. Fig. 3) and (B) shows the ensemble solution (gray lines) in comparison to one of these experimental data sets (blue markers). The purple cross in (A) represents the ensemble spread maximum within experimental accessibility and thus the recommended experiment. (C) illustrates the ensemble solution at this ensemble spread maximum. New experimental data from the recommended experiment (purple markers) are used to obtain the constrained fit ensemble (green lines) through rejection of fits. (D) and (E) showcase ensemble solutions with a high ensemble spread of 1.446 and a low ensemble spread of 0.234, respectively. Here, colored lines visualize the mean of the ensemble solution (blue line) and the mean ± 1 standard deviation (red lines).

solutions (Fig. 1). In this study, we test and compare three different approaches: using KM-SUB for both steps (KM-only), using the SM for both steps (SM-only), and a KM/SM-hybrid approach, in which KM-SUB is used for fit ensemble acquisition and the SM to obtain ensemble solutions.

3 Results and Discussion

3.1 Acquisition of fit ensembles

We demonstrate the applicability of the kinetic compass (KC) for the heterogeneous ozonolysis of oleic acid aerosols using the kinetic multi-layer model of aerosol surface and bulk chemistry (KM-SUB), and a neural network surrogate model (SM) for it. Both models map seven kinetic and

Table 1 KM-SUB kinetic and experimental input parameters. The respective lower and upper boundaries indicate the initial constraints of the fit ensemble and an estimate of experimentally accessible conditions in a laboratory for atmospheric aerosol chemistry.

Parameter	Lower boundary	Upper boundary	Description
k_{SLR}	1.0×10^{-15}	1.0×10^{-8}	Rate coefficient of OL+O_3 surface reaction ($cm^3\ s^{-1}$)
k_{BR}	1.0×10^{-20}	1.0×10^{-11}	Rate coefficient of OL+O_3 bulk reaction ($cm^3\ s^{-1}$)
$D_{\mathrm{b,O3}}$	1.0×10^{-11}	1.0×10^{-5}	Bulk diffusion coefficient of ozone ($cm^2\ s^{-1}$)
$D_{\mathrm{b,OL}}$	1.0×10^{-12}	1.0×10^{-6}	Bulk diffusion coefficient of oleic acid ($cm^2\ s^{-1}$)
$H_{\mathrm{cp,O3}}$	5.0×10^{-6}	5.0×10^{-3}	Henry's law solubility coefficient of ozone ($mol\ cm^{-3}\ atm^{-1}$)
$\tau_{\mathrm{d,O3}}$	1.0×10^{-9}	1.0×10^{-2}	Desorption lifetime of O_3 (s)
$\alpha_{\mathrm{s,0,O3}}$	1.0×10^{-4}	1	Surface accommodation coefficient of ozone on an adsorbate-free surface ( )
r_{p}	2.5×10^{-6}	1.0×10^{-3}	Particle radius (cm)
$[O_3]_{\mathrm{g,0}}$	1.0×10^{11}	1.0×10^{15}	Initial gas phase number concentration of ozone (cm^{-3})
$[\mathrm{OL}]_{\mathrm{b,0}}$	1.0×10^{19}	2.0×10^{21}	Initial bulk number concentration of oleic acid (cm^{-3})

three experimental input parameters (Tab. 1) onto the concentration-time profile of oleic acid. For each model, we obtained fit ensembles (N=500) in compliance with seven experimental data sets [8, 36–38] as shown in Fig. 3. Each kinetic parameter set in the fit ensemble is associated with one model output (gray lines) for each experimental condition. Both fit ensembles (of KM-SUB and the SM) have a minimal mean-squared logarithmic error (MSLE) of 0.0085; the median MSLE are 0.0102 for KM-SUB and 0.0099 for the SM.

3.2 Ensemble spread

Figure 4 displays constraint potential maps for the ensemble spread metric and the variable experimental parameters of particle radius (r_{p}) and ozone concentration ($[O_3]_{\mathrm{g,0}}$). The conditions associated with the experimental data used to obtain the fit ensemble (black crosses) are, naturally, located in areas of low ensemble spread. Maxima of the ensemble spread, i.e. regions associated with large model variance, occur at very low particle radii (< 50 nm), and for the combination of large radii ($> 10\ \mu$m) with high ozone concentrations (> 100 ppm). The constraint potential maps obtained with the KM-only approach (panel A) and the KM/SM-hybrid approach (panel B) appear similar overall. The absolute ensemble spread maxima are both located at maximal particle radii and ozone concentrations (purple crosses). As main difference, isopleths appear less smooth for the SM. A constraint potential map of the SM-only approach is displayed in Fig. S6. The computationally less expensive SM-only method leads to slightly larger differences to the KM-SUB constraint potential map. In particular, the ensemble spread maximum at low particle radii is less pronounced.

3.3 Parameter boundary constraint potential

In addition to the ensemble spread, we apply the KC using both models with the parameter constraint potential (Sec. 2.4). This method aims for a minimization of a chosen kinetic parameter's uncertainty range in the solution space. Figs. 5A and C display parameter constraint potential maps for the kinetic parameters k_{SLR} and $D_{\mathrm{b,OL}}$, respectively. The maximum of the k_{SLR} constraint potential matches the maximum of the ensemble spread at low particle radii in Fig. 4, whereas the maximum of the $D_{\mathrm{b,OL}}$ constraint potential matches the maximum of the ensemble spread at large radii and high ozone concentrations. Hence, high ensemble spreads appear to be necessary but not sufficient conditions for high parameter constraint potentials.

We simulate the suggested experiments with KM-SUB, using the best fit in the KM-SUB fit ensemble as simulated truth. Under consideration of the original data and the new synthetic experiment, we filter the fit ensembles using the MSLE

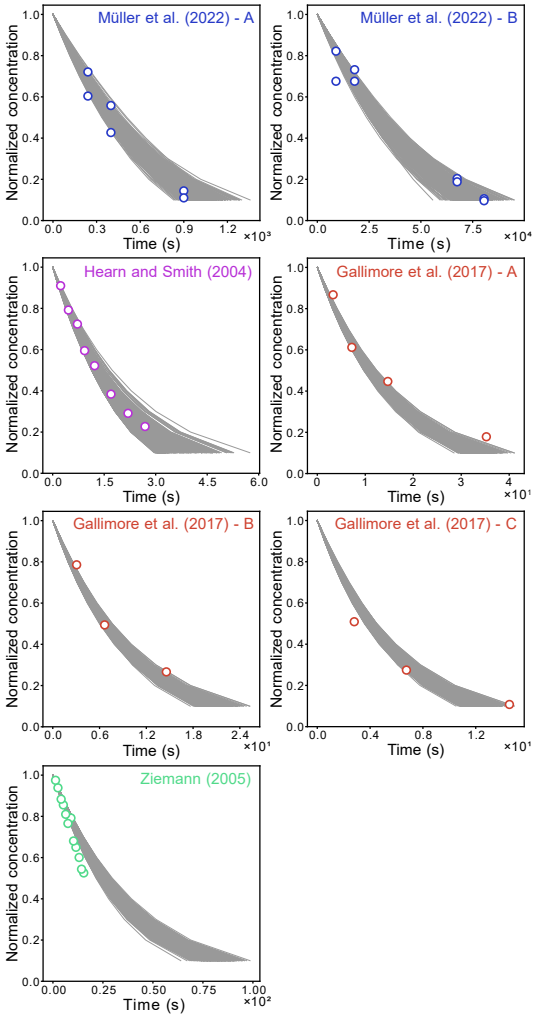

Fig. 3 Ensembles of kinetic multi-layer model of aerosol surface and bulk chemistry (KM-SUB) outputs (N=500, gray lines) with a mean square logarithmic error (MSLE) < 0.0105 in comparison with seven literature data sets (markers) of oleic acid aerosol ozonolysis displayed as normalized oleic acid concentrations ($N_{\mathrm{OL},t}/N_{\mathrm{OL},0}$).

threshold of $\theta = 0.0105$. Figs. 5B and D show frequency distributions of five kinetic parameters in the fit ensemble before (blue) and after (red) fit filtering. The experiments suggested by the constraint potential metrics achieve a significant reduction in the uncertainty range for their associated parameters, k_{SLR} and $D_{\mathrm{b,OL}}$, respectively. Simultaneously, constraints are achieved for other parameters, e.g. k_{BR} in Fig. 5B, following the similarity between the parameter constraint potential maps (Fig. S7). Parameter constraint potential maps and simulated constraints for the SM-only approach (Fig. S8) are very similar to those using the KM-only approach.

3.4 Statistical testing of the kinetic compass method

The KC can be applied repeatedly to narrow down model solutions in iterative fashion. Here, we simulate this procedure using synthetic experimental data, which is obtained by assuming that a single fit from the fit ensemble is the true solution of the modelled system (the *simulated truth*). The simulation is repeated for each fit in the ensemble as simulated truth. Detailed information on the simulation of experimental data is presented in Suppl. Note 7.

Fig. 6 shows the statistics of a total of 500 of these simulations with five iterations of the KC,

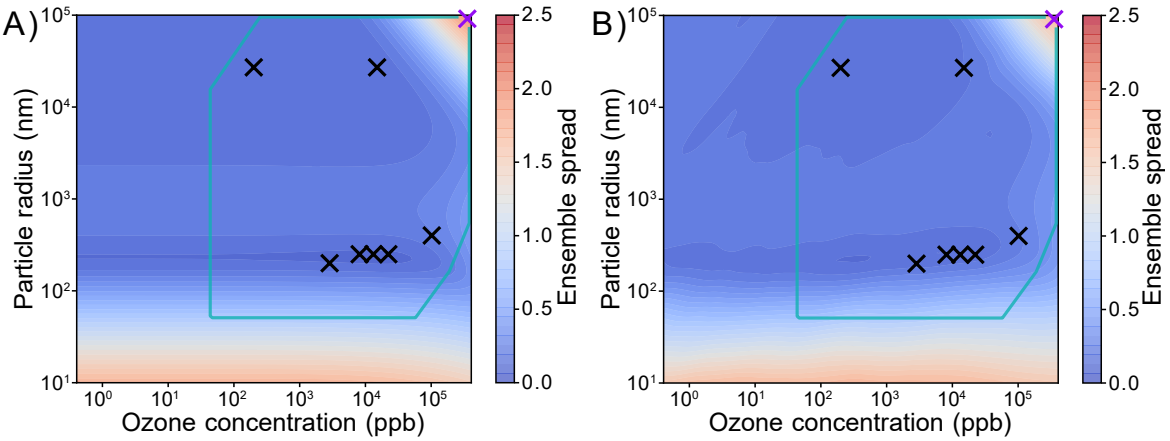

Fig. 4 Constraint potential maps for the ensemble spread, evaluated by (A) KM-SUB (KM-only approach) and (B) SM, based on the KM-SUB fit ensemble (KM/SM-hybrid approach). The teal box outlines conditions for feasible experiments. Black crosses represent the experimental parameters of the seven real experiments that are used for the initial acquisition of the fit ensemble. Purple crosses represent the ensemble spread maximum in each grid with satisfied experimental constraint conditions.

and compares the performance of three numerical experiment selection methods: ensemble spread using KM-SUB (blue), ensemble spread using the KM/SM-hybrid approach (orange), and random selection (green) within the boundaries of experimental accessibility. Fig. 6A shows the decreasing number of accepted fits in the fit ensemble. The median numbers of fits after the five iterations are (121, 49, 38, 31, 28) for the KM-SUB ensemble spread, (121, 53, 39, 35, 29.5) for the KM/SM-hybrid ensemble spread and (421.5, 355, 307, 301, 291) for the random selection. Hence, statistically, the KC leads to a significantly larger constraint of the fit ensemble compared to random selection, irrespective of using the full KM or the SM-assisted hybrid approach. Figs. S10 - S13 show examples of individual trajectories of the KC, i.e. simulations including numerical experiment selection, synthetic experimental data generation, and fit filtering.

4 Conclusion

This study demonstrates the application of computational models to guide experiment design and prioritization based on the anticipated reduction of a model's solution space. The method extrapolates current ensemble solutions to conditions of potential future experiments and identifies conditions under which ensemble variance, and thus model parametric uncertainty is largest. In comparison with random selection, the reduction of fits in the fit ensemble, representing reduction of model variance, is much larger for the kinetic compass (KC) guided numerical selection of experiments.

In our simulations, experiments associated with the maximum of the constraint potential map for the ensemble spread metric led to large constraints of the fit ensemble. However, the same experiments did not achieve a significant constraint of the uncertainty ranges of some kinetic parameters. By evaluating the KC with the parameter constraint potential metric and selecting the experiment accordingly, the constraint of individual parameter uncertainty ranges can be optimized more effectively.

The computational effort of the KC can be strongly reduced by training a neural network surrogate model (SM), with nearly identical results. After consideration of the computational effort of SM training, and for the system at hand, we observe an acceleration of the evaluation of the KC by a factor of $\sim$5 using a KM/SM-hybrid approach, and an acceleration by a factor of $\sim$7.5 using only the SM (Suppl. Note 8). While SM for multiphase kinetic models have already proven useful in forward modelling applications [20], we here further demonstrate their utility in an inverse modelling approach.

For the kinetic multi-layer model of aerosol surface and bulk chemistry (KM-SUB) and the heterogeneous ozonolysis of oleic acid, the KC suggests experiments with either very small particles

($<$ 50 nm) or with exceptionally large particles ($\approx$ 100 µm) and high ozone concentrations ($\approx$ 1000 ppm) (Sec. 3.2). The first suggestion seems logical: experiments with nano-sized particles of oleic acid have not been conducted and extrapolation to these conditions will be associated with model uncertainty. The method predicts that measurements using nano-sized particles would help especially to constrain the surface reaction rate coefficient k_{SLR}. The second suggestion of the KC may seem counter-intuitive, as these large particle - high ozone conditions are far away from atmospheric relevance. In fact, these experiments likely offer a constraint on the diffusion coefficient of oleic acid, $D_{\mathrm{b,OL}}$, a parameter that is rather unimportant under typical atmospheric conditions. Note, however, that the simple model used in this analysis does not consider changes in $D_{\mathrm{b,OL}}$ upon formation of oxidation products.

Overall, this analysis of the oleic acid - ozone reaction system shows that additional experiments measuring the loss of oleic acid under conditions typical for the atmosphere will not improve our knowledge of this well-studied system any further. More extreme conditions are needed to narrow down the model solution space, however, this will not come with an improvement of the predictive power of our models for atmospheric conditions (other than small nano-particles). Conversely, any solution in the fit ensemble obtained in this study and in Berkemeier et al. 2021 [19] should perform well under atmospherically-relevant conditions. More knowledge about the system can also be derived by changing the experimental observable. For the heterogeneous ozonolysis of alkenes, for example, product analyses have recently provided additional constraints for kinetic models [38, 39]. Extending the KC method from experimental conditions to experimental observables will be a subject of future studies.

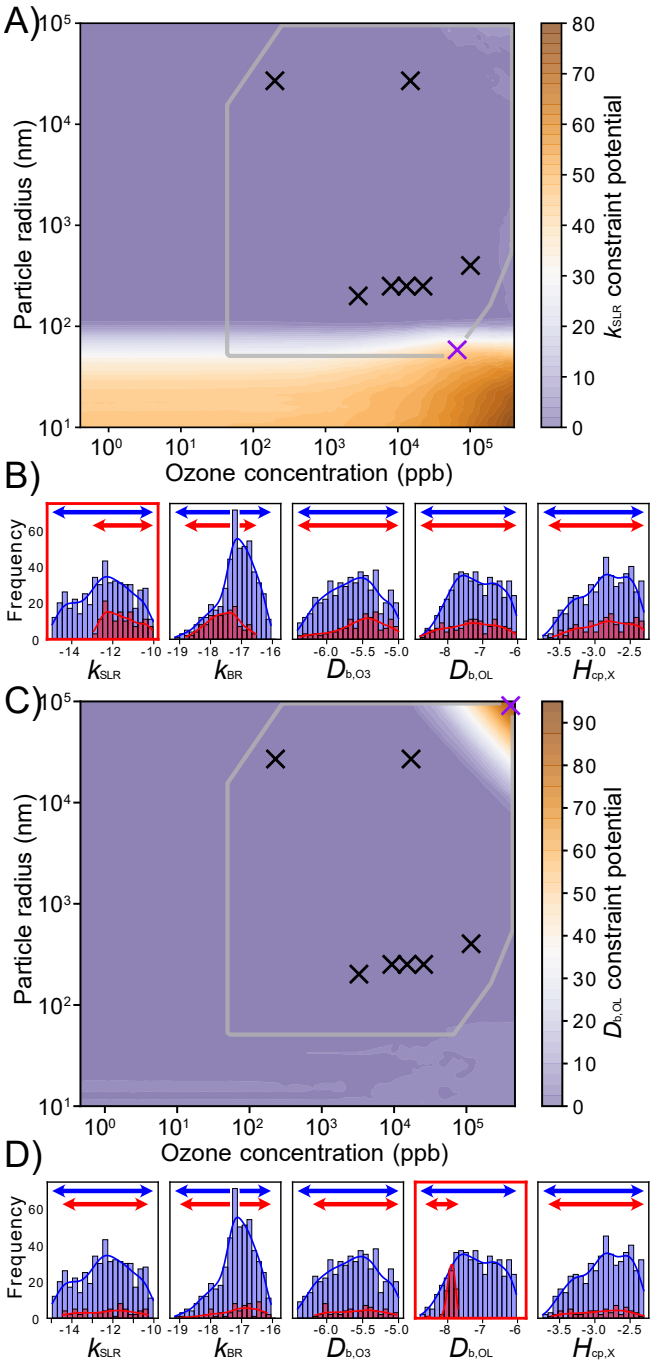

Fig. 5 Constraint potential maps for the kinetic parameters (A) k_{SLR} and (C) $D_{\mathrm{b,OL}}$ obtained with KM-SUB. The gray box outlines conditions for feasible experiments. Black crosses represent the experimental parameter sets of the seven real experiments that are used for the initial acquisition of the fit ensemble. The purple cross represents the parameter constraint potential maximum with satisfied experimental constraint conditions. The suggested experimental conditions are used to obtain synthetic experimental data by evaluating KM-SUB for the best fit in the KM-SUB fit ensemble. Frequency distributions of five kinetic parameters are shown and highlighted for (B) k_{SLR} and (D) $D_{\mathrm{b,OL}}$ in the KM-SUB fit ensemble before (blue) and after (red) fit filtering with error threshold $\theta = 0.0105$. Blue and red arrows visualize the outer boundaries of each distribution.

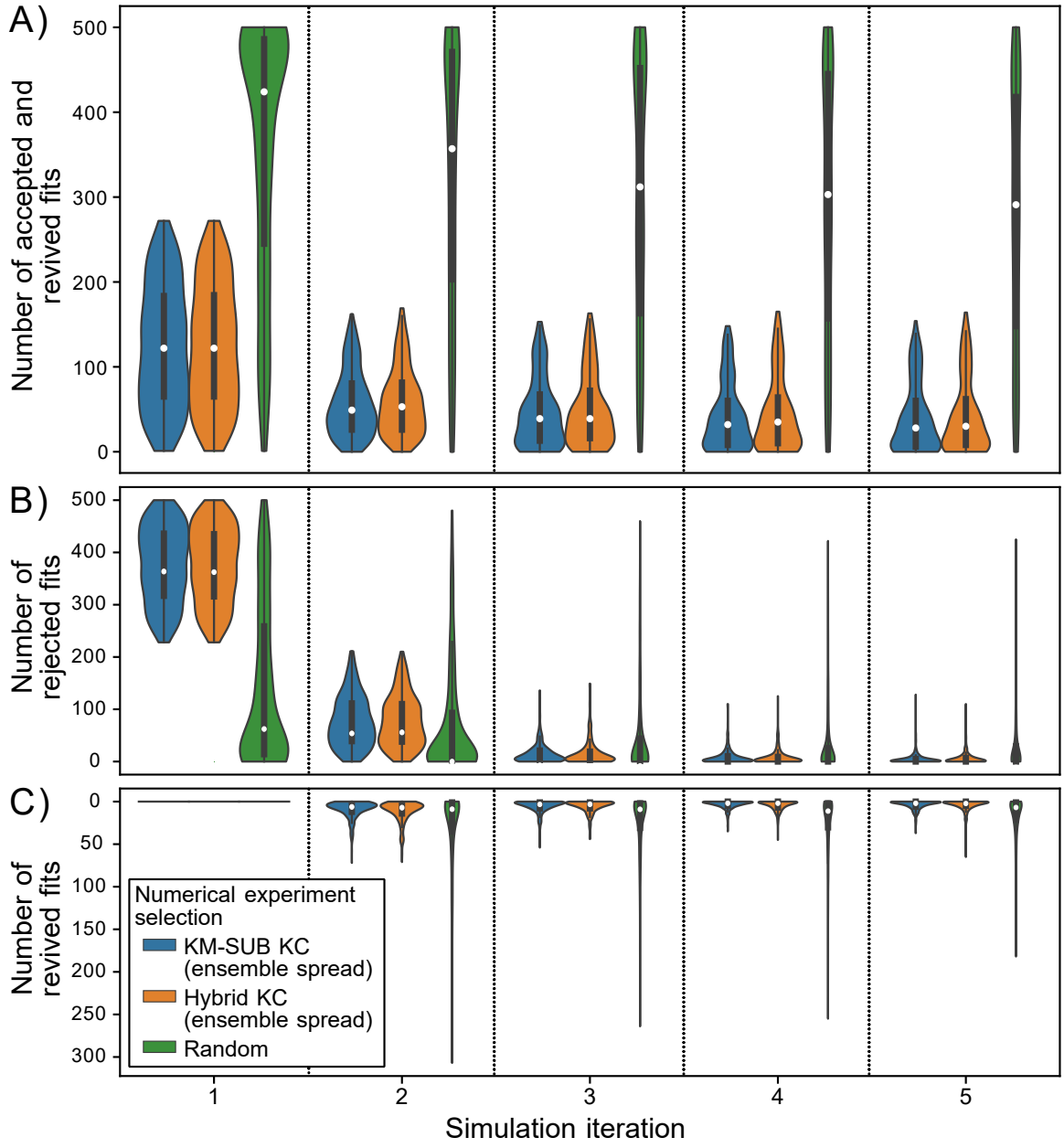

Fig. 6 Number of fits that are (A) accepted, (B) rejected and (C) revived based on synthetic experimental data in five iterations of the kinetic compass (KC). Numbers are based on statistics for $n = 500$ simulations, where each fit in the KM-SUB fit ensemble is once selected as simulated truth. Medians are shown as white markers, interquantile ranges as vertical wide black lines and 1.5 $\times$ interquantile ranges as narrow black lines. While experiment simulation (via KM-SUB) and fit filtering (of the KM-SUB fit ensemble, absolute MSLE threshold, $\theta = 0.0105$) are identical for all approaches, we compare different numerical selection methods of experiments: KM-only KC (blue), KM/SM-hybrid KC (orange), and random selection of experiments (green). Fit ensemble constraint is significantly larger when experiments are selected using the KC. While the two models utilized for its evaluation lead to very similar fit ensemble constraints, the random selection of experiments performs significantly worse.

List of Abbreviations. CP - (parameter boundary) constraint potential
ENS - ensemble solution
ES - ensemble spread
FE - fit ensemble
KC - kinetic compass
KM - kinetic model
KM-SUB - kinetic multi-layer model of aerosol surface and bulk chemistry
MSLE - mean-squared logarithmic error
OL - oleic acid
SM - surrogate model

Supplementary information. The online version contains supplementary material available at t https://doi.org/....

Additional file 1: Suppl. Note 1. Equations for process models, fit ensembles and prediction ensembles. **Suppl. Note 2.** Fit ensemble acquisition with KM-SUB and SM. **Suppl. Note 3.** Equations for ensemble mean and standard deviation. **Suppl. Note 4.** Parameter boundary constraint potential metric with reduced sample density. **Suppl. Note 5.** Oleic acid ozonolysis system applied in this study. **Suppl. Note 6.** Surrogate model training. **Suppl. Note 7.** Uncertainty calibration and simulated experiments. **Suppl. Note 8.** Computational effort. **Figure S1.** Contrariwise cross-evaluation of the KM-SUB and SM fit ensembles. **Figure S2.** Scatter plot matrix of the KM-SUB fit ensemble. **Figure S3.** Scatter plot matrix of the SM fit ensemble. **Figure S4.** Visualization of the parameter constraint potential metric. **Figure S5.** Restrictions for constraint potential maps with regards to experimental feasibility. **Figure S6.** Constraint potential maps for the ensemble spread, evaluated by KM-SUB and SM. **Figure S7.** Parameter constraint potential maps evaluated by KM-SUB and the SM. **Figure S8.** Parameter constraint potential maps evaluated by KM-SUB and the SM. **Figure S9.** Visualization of the uncertainty calibration method. **Figure S10.** Simulated trajectories for iterative KC application. **Figure S11.** Simulated trajectories for iterative KC application. **Figure S12.** Simulated trajectories for iterative KC application. **Figure S13.** Simulated trajectories for iterative KC application.

Acknowledgments. The authors thank Coraline Mattei for helpful discussions. Parts of this research were conducted using the supercomputer Mogon and/or advisory services offered by Johannes Gutenberg University Mainz (hpc.uni-mainz.de), which is a member of the AHRP (Alliance for High Performance Computing in Rhineland Palatinate, www.ahrp.info) and the Gauss Alliance e.V. The authors gratefully acknowledge the computing time granted on the supercomputer Mogon at Johannes Gutenberg University Mainz (hpc.uni-mainz.de).

Authors' contributions. TB conceived the study. MK and TB designed research. TB wrote the kinetic model code and performed simulations. MK wrote the kinetic compass and surrogate model code and performed simulations. All authors discussed and interpreted calculation results. MK and TB wrote the manuscript with contributions from all authors.

Funding. This work was funded by the Max Planck Society (MPG). AM and MK are supported by the Max Planck Graduate Center with the Johannes Gutenberg University Mainz (MPGC).

Availability of data and materials. The data is openly available at https://doi.org/10.17617/3.D5PCQK.

Code availability. The source code is openly available at https://doi.org/10.17617/3.D5PCQK. The kinetic compass is available as package for the programming language Julia at https://gitlab.mpcdf.mpg.de/mkruege/kineticcompass.

Declarations

Competing interests. The authors declare that they have no competing interests.

Ethical approval and consent to participate. Not applicable.

References

[1] Worsnop, D.R., Morris, J.W., Shi, Q., Davidovits, P., Kolb, C.E.: A chemical kinetic model for reactive transformations of aerosol particles: Reactive transformation of aerosol particles. Geophys. Res. Lett.

29(20), 57–1574 (2002) https://doi.org/10.1029/2002GL015542

[2] Pöschl, U., Rudich, Y., Ammann, M.: Kinetic model framework for aerosol and cloud surface chemistry and gas-particle interactions – Part 1: General equations, parameters, and terminology. Atmos. Chem. Phys. **7**(23), 5989–6023 (2007) https://doi.org/10.5194/acp-7-5989-2007

[3] Kolb, C.E., Cox, R.A., Abbatt, J.P.D., Ammann, M., Davis, E.J., Donaldson, D.J., Garrett, B.C., George, C., Griffiths, P.T., Hanson, D.R., Kulmala, M., McFiggans, G., Pöschl, U., Riipinen, I., Rossi, M.J., Rudich, Y., Wagner, P.E., Winkler, P.M., Worsnop, D.R., O' Dowd, C.D.: An overview of current issues in the uptake of atmospheric trace gases by aerosols and clouds. Atmos. Chem. Phys. **10**(21), 10561–10605 (2010) https://doi.org/10.5194/acp-10-10561-2010

[4] Abbatt, J.P.D., Lee, A.K.Y., Thornton, J.A.: Quantifying trace gas uptake to tropospheric aerosol: recent advances and remaining challenges. Chem. Soc. Rev. **41**, 6555–6581 (2012) https://doi.org/10.1039/C2CS35052A

[5] Shiraiwa, M., Pfrang, C., Pöschl, U.: Kinetic multi-layer model of aerosol surface and bulk chemistry (KM-SUB): the influence of interfacial transport and bulk diffusion on the oxidation of oleic acid by ozone. Atmos. Chem. Phys. **10**(8), 3673–3691 (2010) https://doi.org/10.5194/acp-10-3673-2010

[6] Shiraiwa, M., Pfrang, C., Koop, T., Pöschl, U.: Kinetic multi-layer model of gas-particle interactions in aerosols and clouds (KM-GAP): linking condensation, evaporation and chemical reactions of organics, oxidants and water. Atmos. Chem. Phys. **12**(5), 2777–2794 (2012) https://doi.org/10.5194/acp-12-2777-2012

[7] Roldin, P., Eriksson, A.C., Nordin, E.Z., Hermansson, E., Mogensen, D., Rusanen, A., Boy, M., Swietlicki, E., Svenningsson, B., Zelenyuk, A., Pagels, J.: Modelling non-equilibrium secondary organic aerosol formation and evaporation with the aerosol dynamics, gas- and particle-phase chemistry kinetic multilayer model ADCHAM. Atmos. Chem. Phys. **14**(15), 7953–7993 (2014) https://doi.org/10.5194/acp-14-7953-2014

[8] Gallimore, P.J., Griffiths, P.T., Pope, F.D., Reid, J.P., Kalberer, M.: Comprehensive modeling study of ozonolysis of oleic acid aerosol based on real-time, online measurements of aerosol composition: Organic Aerosol Model and Measurements. J. Geophys. Res. Atmos. **122**(8), 4364–4377 (2017) https://doi.org/10.1002/2016JD026221

[9] Wilson, K.R., Prophet, A.M., Willis, M.D.: A kinetic model for predicting trace gas uptake and reaction. J. Phys. Chem. A **126**(40), 7291–7308 (2022) https://doi.org/10.1021/acs.jpca.2c03559 https://doi.org/10.1021/acs.jpca.2c03559. PMID: 36170058

[10] Milsom, A., Lees, A., Squires, A.M., Pfrang, C.: MultilayerPy (v1.0): a Python-based framework for building, running and optimising kinetic multi-layer models of aerosols and films. Geosci. Model Dev. **15**(18), 7139–7151 (2022) https://doi.org/10.5194/gmd-15-7139-2022

[11] Tsuchiya, M., Ross, J.: Application of Genetic Algorithm to Chemical Kinetics: Systematic Determination of Reaction Mechanism and Rate Coefficients for a Complex Reaction Network. J. Phys. Chem. A **105**(16), 4052–4058 (2001) https://doi.org/10.1021/jp004439p

[12] Berkemeier, T., Huisman, A.J., Ammann, M., Shiraiwa, M., Koop, T., Pöschl, U.: Kinetic regimes and limiting cases of gas uptake and heterogeneous reactions in atmospheric aerosols and clouds: a general classification scheme. Atmos. Chem. Phys. **13**(14), 6663–6686 (2013) https://doi.org/10.5194/acp-13-6663-2013

[13] Taylor, C.J., Booth, M., Manson, J.A., Willis,

M.J., Clemens, G., Taylor, B.A., Chamberlain, T.W., Bourne, R.A.: Rapid, automated determination of reaction models and kinetic parameters. Chem. Eng. J. **413**, 127017 (2021) https://doi.org/10.1016/j.cej.2020.127017

[14] Willis, M.D., Wilson, K.R.: Coupled Interfacial and Bulk Kinetics Govern the Timescales of Multiphase Ozonolysis Reactions. J. Phys. Chem. A **126**(30), 4991–5010 (2022) https://doi.org/10.1021/acs.jpca.2c03059

[15] Berkemeier, T., Ammann, M., Krieger, U.K., Peter, T., Spichtinger, P., Pöschl, U., Shiraiwa, M., Huisman, A.J.: Technical note: Monte Carlo genetic algorithm (MCGA) for model analysis of multiphase chemical kinetics to determine transport and reaction rate coefficients using multiple experimental data sets. Atmos. Chem. Phys. **17**(12), 8021–8029 (2017) https://doi.org/10.5194/acp-17-8021-2017

[16] Tikkanen, O.-P., Hämäläinen, V., Rovelli, G., Lipponen, A., Shiraiwa, M., Reid, J.P., Lehtinen, K.E.J., Yli-Juuti, T.: Optimization of process models for determining volatility distribution and viscosity of organic aerosols from isothermal particle evaporation data. Atmos. Chem. Phys. **19**(14), 9333–9350 (2019) https://doi.org/10.5194/acp-19-9333-2019

[17] Wei, J., Fang, T., Lakey, P.S.J., Shiraiwa, M.: Iron-Facilitated Organic Radical Formation from Secondary Organic Aerosols in Surrogate Lung Fluid. Environ. Sci. Technol. **56**(11), 7234–7243 (2022) https://doi.org/10.1021/acs.est.1c04334

[18] Milsom, A., Squires, A.M., Ward, A.D., Pfrang, C.: The impact of molecular self-organisation on the atmospheric fate of a cooking aerosol proxy. Atmos. Chem. Phys. **22**(7), 4895–4907 (2022) https://doi.org/10.5194/acp-22-4895-2022

[19] Berkemeier, T., Mishra, A., Mattei, C., Huisman, A.J., Krieger, U.K., Pöschl, U.: Ozonolysis of Oleic Acid Aerosol Revisited: Multiphase Chemical Kinetics and Reaction Mechanisms. ACS Earth Space Chem. **5**(12), 3313–3323 (2021) https://doi.org/10.1021/acsearthspacechem.1c00232

[20] Berkemeier, T., Krüger, M., Feinberg, A., Müller, M., Pöschl, U., Krieger, U.K.: Accelerating models for multiphase chemical kinetics through machine learning with polynomial chaos expansion and neural networks. Geosci. Model Dev. **16**(7), 2037–2054 (2023) https://doi.org/10.5194/gmd-16-2037-2023

[21] O'Gorman, P.A., Dwyer, J.G.: Using Machine Learning to Parameterize Moist Convection: Potential for Modeling of Climate, Climate Change, and Extreme Events. J. Adv. Model. Earth Syst. **10**(10), 2548–2563 (2018) https://doi.org/10.1029/2018MS001351

[22] Rasp, S., Pritchard, M.S., Gentine, P.: Deep learning to represent subgrid processes in climate models. Proc. Natl. Acad. Sci. U.S.A. **115**(39), 9684–9689 (2018) https://doi.org/10.1073/pnas.1810286115

[23] Keller, C.A., Evans, M.J.: Application of random forest regression to the calculation of gas-phase chemistry within the GEOS-Chem chemistry model v10. Geosci. Model Dev. **12**(3), 1209–1225 (2019) https://doi.org/10.5194/gmd-12-1209-2019

[24] Lu, D., Ricciuto, D.: Efficient surrogate modeling methods for large-scale Earth system models based on machine-learning techniques. Geosci. Model Dev. **12**(5), 1791–1807 (2019) https://doi.org/10.5194/gmd-12-1791-2019

[25] Kelp, M.M., Jacob, D.J., Kutz, J.N., Marshall, J.D., Tessum, C.W.: Toward Stable, General Machine-Learned Models of the Atmospheric Chemical System. J. Geophys. Res. Atmos. **125**(23) (2020) https://doi.org/10.1029/2020JD032759

[26] Harder, P., Watson-Parris, D., Stier, P., Strassel, D., Gauger, N.R., Keuper, J.: Physics-informed learning of aerosol microphysics. Environ. Data Science **1**, 20 (2022) https://doi.org/10.1017/eds.2022.22

[27] Sturm, P.O., Wexler, A.S.: Conservation laws in a neural network architecture: enforcing the atom balance of a Julia-based photochemical model (v0.2.0). Geosci. Model Dev. **15**(8), 3417–3431 (2022) https://doi.org/10.5194/gmd-15-3417-2022

[28] McBride, K., Sundmacher, K.: Overview of Surrogate Modeling in Chemical Process Engineering. Chem. Ing. Tech. **91**(3), 228–239 (2019) https://doi.org/10.1002/cite.201800091

[29] Yan, S., Minsker, B.: Applying Dynamic Surrogate Models in Noisy Genetic Algorithms to Optimize Groundwater Remediation Designs. J. Water Resour. Plann. Manage. **137**(3), 284–292 (2011) https://doi.org/10.1061/(ASCE)WR.1943-5452.0000106

[30] Razavi, S., Tolson, B.A., Burn, D.H.: Review of surrogate modeling in water resources. Water Resour. Res. **48**(7) (2012) https://doi.org/10.1029/2011WR011527

[31] Wan, X., Pekny, J.F., Reklaitis, G.V.: Simulation-based optimization with surrogate models—Application to supply chain management. Comput. Chem. Eng. **29**(6), 1317–1328 (2005) https://doi.org/10.1016/j.compchemeng.2005.02.018

[32] Franceschini, G., Macchietto, S.: Model-based design of experiments for parameter precision: State of the art. Chem. Eng. Sci. **63**(19), 4846–4872 (2008) https://doi.org/10.1016/j.ces.2007.11.034

[33] Hu, Z., Ao, D., Mahadevan, S.: Calibration experimental design considering field response and model uncertainty. Comput. Methods Appl. Mech. Eng. **318**, 92–119 (2017) https://doi.org/10.1016/j.cma.2017.01.007

[34] Jung, Y., Lee, I.: Optimal design of experiments for optimization-based model calibration using Fisher information matrix. Reliab. Eng. Syst. Saf. **216**, 107968 (2021) https://doi.org/10.1016/j.ress.2021.107968

[35] Whitaker, J.S., Loughe, A.F.: The relationship between ensemble spread and ensemble mean skill. Mon. Weather Rev. **126**(12), 3292–3302 (1998) https://doi.org/10.1175/1520-0493(1998)126⟨3292:TRBESA⟩2.0.CO;2

[36] Hearn, J.D., Smith, G.D.: Kinetics and Product Studies for Ozonolysis Reactions of Organic Particles Using Aerosol CIMS. J. Phys. Chem. A **108**(45), 10019–10029 (2004) https://doi.org/10.1021/jp0404145

[37] Ziemann, P.J.: Aerosol products, mechanisms, and kinetics of heterogeneous reactions of ozone with oleic acid in pure and mixed particles. Faraday Discuss. **130**, 469 (2005) https://doi.org/10.1039/b417502f

[38] Müller, M., Mishra, A., Berkemeier, T., Hausammann, E., Peter, T., Krieger, U.K.: Electrodynamic balance–mass spectrometry reveals impact of oxidant concentration on product composition in the ozonolysis of oleic acid. Phys. Chem. Chem. Phys. **24**(44), 27086–27104 (2022) https://doi.org/10.1039/D2CP03289A

[39] Reynolds, R., Ahmed, M., Wilson, K.R.: Constraining the reaction rate of criegee intermediates with carboxylic acids during the multiphase ozonolysis of aerosolized alkenes. ACS Earth Space Chem. **7**(4), 901–911 (2023) https://doi.org/10.1021/acsearthspacechem.3c00026

Supplementary Files

This is a list of supplementary files associated with this preprint. Click to download.

- KruegerKineticCompassSI.pdf